Available online at www.sciencedirect.com

ScienceDirect

Acta Materialia 61 (2013) 7555–7567

Acta MATERIALIA

www.elsevier.com/locate/actamat

Methodology for estimating the critical resolved shear stress ratios of α-phase Ti using EBSD-based trace analysis

H. Li [a], D.E. Mason [b], T.R. Bieler [a], C.J. Boehlert [a,*], M.A. Crimp [a]

[a] Department of Chemical Engineering and Materials Science, Michigan State University, East Lansing, MI 48824, USA
[b] Department of Mathematics and Computer Science, Albion College, Albion, MI 49224, USA

Received 8 July 2013; received in revised form 20 August 2013; accepted 21 August 2013
Available online 28 September 2013

Abstract

A novel method for calculating the critical resolved shear stress (CRSS) ratios of different deformation system types in polycrystalline non-cubic metals has been developed. The mean CRSS ratios between different deformation systems were calculated for both commercially pure (CP) Ti and Ti–5Al–2.5Sn (wt.%) tensile deformed at ambient temperature and 455 °C using an in situ scanning electron microscope-based testing technique combined with electron backscattered diffraction. It was found that the relative activity of the different deformation systems changes as a function of alloying composition and deformation temperature. Prismatic slip was the most active deformation mode for CP Ti. CP Ti exhibited a lower resistance to prismatic slip at both ambient and elevated temperatures compared with Ti–5Al–2.5Sn. For Ti–5Al–2.5Sn, prismatic slip was the most active deformation system at ambient temperature although the basal slip activity significantly increased compared to CP Ti, mostly likely due to an increased *c/a* ratio resulting in a closer packed basal plane. At 455 °C, basal slip exhibited a lower CRSS than prismatic slip for Ti–5Al–2.5Sn. The relative activity of other deformation systems was also affected by alloying and temperature. The statistical resampling technique of bootstrapping was used to generate multiple equivalent data sets from which mean CRSS ratios between different deformation systems, and associated confidence intervals, could be deduced. It was found that the mean CRSS ratios at low and high strains varied slightly for the same testing conditions. Moreover, lesser activated slip systems resulted in relatively larger confidence intervals for the CRSS means. This variability may be attributed to a number of potential factors, including measurement errors, rotations of grains during deformation, local stress state variations, and work hardening. The analysis further suggests that awareness of the intrinsic statistical variability in CRSS ratios should be considered when formulating crystal plasticity constitutive models.

Keywords: Titanium; Schmid factor; Critical resolved shear stress; Deformation behavior; Tension

1. Introduction

The deformation mechanisms of hexagonal α Ti and hexagonal α Ti alloys have been studied over the past few decades [1–26]. Generally, there are three slip systems with a $\langle \bar{2}110 \rangle$ Burgers vector (a-type), which have been observed to slip on basal $\{0001\}$, prismatic $\{10\bar{1}0\}$, and first-order pyramidal $10\bar{1}1\}$ planes. According to the von Mises criterion [27], five independent slip systems are required to accommodate any arbitrary shape change during plastic deformation. Thus, in addition to the three a-type slip systems, additional non a-type deformation mechanisms must be activated in order to allow the arbitrary shape changes of a grain that is usually necessary to maintain polycrystalline compatibility. Pyramidal $\langle c + a \rangle$ dislocation slip as well as four α-phase twinning systems – $\{10\bar{1}2\}\langle\bar{1}011\rangle$ T1 tensile twinning, $\{11\bar{2}1\}\langle\bar{1}\bar{1}26\rangle$ T2 tensile twinning, $\{11\bar{2}2\}\langle11\bar{2}\bar{3}\rangle$ C1 compressive twinning and $\{10\bar{1}1\}\langle10\bar{1}2\rangle$ C2 compressive twinning [23] – have been reported that can meet this requirement. Of these, pyramidal $\langle c + a \rangle$ and $\{10\bar{1}2\}\langle\bar{1}011\rangle$ T1 tensile twinning are most commonly

* Corresponding author.
E-mail address: boehlert@egr.msu.edu (C.J. Boehlert).

1359-6454/$36.00 © 2013 Acta Materialia Inc. Published by Elsevier Ltd. All rights reserved.
http://dx.doi.org/10.1016/j.actamat.2013.08.042

reported for room temperature (RT) deformation in commercially pure (CP) Ti.

The ease of slip or twinning on a particular system is quantified by the critical resolved shear stress (CRSS). Researchers have investigated the CRSS or the CRSS ratios of Ti and Ti alloys under various conditions, both experimentally and computationally [5–22]. However, there is no consensus on these values or ratios, particularly as they change as a function of alloy content and testing conditions. Table 1 shows a number of reported values for the CRSS and/or CRSS ratios for slip systems at RT and elevated temperatures for Ti and Ti alloys [5–22]. This shows significant variation in these values, even for the same nominal alloys under the same deformation temperatures and test conditions. For CP Ti, although the CRSS values measured at ambient temperature vary significantly, there is general agreement that prismatic slip is easier to activate than other deformation modes, and that basal slip is more easily activated than pyramidal $\langle c + a \rangle$ slip [3–7,24–26,28]. Conrad [25] and Akhtar and Teghtsoonian [26] both found that this trend continued up to 827 °C. Table 1 also indicates that compared with CP Ti, alloys with Al additions have increased CRSS for both basal and prismatic slip systems. For CP Ti, the CRSS of basal and prismatic slip were measured to be 209 and 181 MPa [5], respectively, but increased to 373 and 388 MPa for Ti–6Al–4V [14] and 275.8 and 206.9 MPa for Ti–8Al–1Mo–1V [22].

The relative activity of basal and prismatic slip also changes with alloying [21]. However, there have been conflicting reports on how the activity of prismatic and basal slip systems is affected by alloying. This is illustrated for Ti–6Al–4V alloys, where in some cases, the CRSS of basal slip has even been found to be lower than that of prismatic slip [14]. However, others have reported that basal slip exhibits a higher CRSS than prismatic in Ti–6Al–4V at both 22 °C [12,13,15,16] and between 815 and 955 °C [19]. Temperature also plays a role in the relative activation of basal and prismatic slip systems. Williams et al. [21] showed that increasing temperature leads to a decrease in the CRSS for the basal and prismatic slip systems for single-crystal α Ti–Al alloys with compositions ranging from Ti–1.4Al to Ti–6.6Al. However, this decrease was more dramatic for the basal slip systems.

Much of the uncertainty in the CRSS and CRSS ratios in these Ti alloys can be attributed to the difficulty in directly measuring these parameters in non-cubic metals using traditional single-crystal approaches. To date, CRSS values and ratios have been measured using single crystals for CP Ti [5–6], Ti–1.4Al [21], Ti–2.9Al [21], Ti–5Al [21], Ti–6Al–4V [12] and Ti–6.6Al [21] at temperatures ranging from 22 to 727 °C. However, depending on the relative CRSS values, it is not always possible to determine these values for all slip systems using conventional uniaxial tests. This is because even with high Schmid factors it can be difficult or impossible to initiate slip on some systems if the CRSS is much lower on other systems. Furthermore, many commercial structural metals are polycrystalline and/or multiphase materials and are often not available in single-crystal form, making traditional approaches difficult.

A number of alternative approaches have been taken to determine CRSS values. Nanoindentation of grains within a polycrystal combined with crystal plasticity finite-element simulations has been used to quantitatively determine the CRSS for different slip systems for CP Ti [30,31]. By optimizing the simulations of the nanoindentation behavior in different grains with different orientations, CRSS values have been determined using an optimization procedure by constraining the CRSS values to generate the topographic results measured experimentally.

Although the activation of deformation systems in polycrystals is complicated by the constraints associated with neighboring grains, studying polycrystalline deformation may provide a means for understanding deformation systems that are difficult to activate. A viscoplastic self-consistent model has been used to study the deformation of Ti alloys and determine the CRSS values [17,18]. However, even for a simplified model, simulations require a vast number of computations, limiting the technique. Using a global stress state tensor, Zaefferer [7] calculated the relative resolved shear stresses for the different deformation systems for CP Ti without simulations. Zaefferer also estimated the upper bound of the CRSS ratios of different slip systems by calculating the ratios of the Schmid factors of activated and non-activated slip systems [7]. The relative CRSSs were determined for individual grains with visible slip bands, based on the Schmid factors of the activated slip system and each inactivated slip system. Different CRSS ratios were obtained from different grains with different orientations, showing significant variations in the relative CRSSs.

In the present study, instead of calculating the CRSS ratios for individual grains, an optimization methodology is developed to compute the CRSS ratios. This technique minimizes the difference between the observed and expected number of observations (accounting for texture) of activated deformation systems in all of the grains from a given microstructure patch. This calculation provides one set of CRSS ratios for a given testing condition and given microstructural patch, and with statistical analysis, the confidence of this set of computed CRSS values is assessed. The confidence in this method depends on the assumption that the large number of slip observations in about 200 grains is sufficient to represent the average behavior of a material, and thereby overcome the fact that the local stress tensor in some grains (or parts of grains) can differ significantly from a global uniaxial stress tensor.

2. Materials and experimental procedures

Fully-α CP Ti and near-α Ti–5Al–2.5Sn were investigated in this study. The bulk compositions of the CP Ti and Ti–5Al–2.5Sn were measured using optical emission spectroscopy and inductively coupled plasma mass

Table 1
List of the CRSS (in MPa) and CRSS ratios (relative values) of slip systems in single-crystal and polycrystalline Ti and Ti alloys. E, experimental; S, simulated.

Materials/testing method	Basal	Prismatic	Pyramidal ⟨a⟩	Pyramidal ⟨c + a⟩	Ref.
Single-crystal Ti^{E}	209 MPa	181 MPa		474 MPa	[5]
Single-crystal Ti^{E}	1	0.8		2.1	[6]
Polycrystal CP Ti^{E}		1		13 (upper bond)	[7]
Polycrystal CP Ti (RT)^{S}	150 MPa	30 MPa		120 MPa	[8]
Polycrystal CP Ti (RT)^{S}	3.1 MPa	4.2 MPa		12 MPa	[9]
Polycrystal CP Ti (RT)^{S}	49 MPa	37 MPa		197 MPa	[10]
Polycrystal Ti (750 °C)^{S}	1	1	1	10	[1,11]
Single-crystal Ti64 (RT)^{E}	444 MPa (compression)	376 MPa (tension) 392 MPa (compression)	404 MPa (compression)	441 MPa (tension) 631 MPa (compression)	[12]
Polycrystal Ti64 (RT)^{E}	494 MPa (tension) 513 MPa (compression)	395 MPa	395 MPa	494 MPa (tension) 612 MPa (compression)	[13]
Polycrystal Ti64(RT)^{E}	373 MPa	388 MPa			[14]
Polycrystal Ti64(RT)^{S}	400 MPa	380 MPa		640 MPa	[15]
Polycrystal Ti64 (RT)^{S}	3–6	1	3–6	4–10	[16]
Polycrystal Ti64 (RT)^{S}	1	0.67	2	0.67	[17]
Polycrystal Ti64 (RT)^{S}	1	1	8		[18]
Polycrystal Ti64 (815–955 °C)^{E}	1	0.7		3	[19]
Polycrystal Ti6246 (RT)^{S}	380 MPa			615 MPa	[20]
Single-crystal Ti–6.6Al (RT)^{E}	~1	~1			[21]
Polycrystal Ti8Al1Mo1V (RT)^{E}	275.8 MPa	206.9 MPa	248.2 MPa		[22]

spectroscopy, with the results shown in Table 2. Fig. 1 shows representative scanning electron microscopy (SEM) images of the as-received CP Ti and Ti–5Al–2.5Sn microstructures. The average hexagonal close-packed (hcp) α grain sizes of the CP Ti and the Ti–5Al–2.5Sn were 115 and 45 μm, respectively, measured by the line-intercept method [29]. For Ti–5Al–2.5Sn, the body-centered cubic (bcc) β phase was observed at some of the equiaxed α-phase grain boundaries and consisted of <1% of the specimen volume as measured on SEM images using Image J software [32]. Due to its small volume fraction, this phase was ignored in the deformation mode analysis.

Both materials exhibited a weak texture with a maximum peak intensity of ~3–4 times random, which has been reported in Ref. [28]. In situ tensile testing was performed for both the CP Ti and Ti–5Al–2.5Sn at 22 and 455 °C, resulting in a total of four tests. A more detailed description of the experimental procedure can be found in Ref. [28]. Electron backscattered diffraction (EBSD) was performed both before and after the deformation. Slip/twin trace analysis was used to identify the activation of the different slip and twinning modes as a function of temperature and the global stress state Schmid factor. The number of observations of a given deformation system type (i.e. basal, prismatic, pyramidal ⟨a⟩, pyramidal ⟨c + a⟩ and twinning) and a given global Schmid factor range under different testing conditions for both CP Ti and Ti–5Al–2.5Sn were also reported in Ref. [28]. Regarding the observations of slip on pyramidal planes, there are three slip directions (two ⟨c + a⟩ and one ⟨a⟩). Of the three, the one with the highest Schmid factor was associated with the slip trace. Only the T1 twinning systems were observed in this study.

3. Analysis methodology

3.1. Experimentally observed deformation system activation distribution

For each of the experimental condition combinations of alloy composition and deformation temperature, the deformation system activity is recorded as a function of deformation system type (as identified by trace analysis) and the Schmid factor based on an assumption of a uniaxial global stress state. An example of this data distribution is shown in Table 3, which shows the number of observations of each of the five deformation system types (i.e. basal, prismatic, pyramidal ⟨a⟩, pyramidal ⟨c + a⟩ and T1 twinning) and the correlated global Schmid factor at ambient temperature. The number of observed deformation systems is binned based on Schmid factor increments of 0.05, so there are 10 Schmid factor bins for each of the five deformation system types. This defines a matrix where the value for each pair (i,j) is denoted as N_{ij} $(i = 1,\ldots,10,$ $j = 1,\ldots,5)$. This table is termed the deformation system–Schmid factor distribution. This table is populated based on the number of instances that each combination of deformation system and Schmid factor is observed on a grain-by-grain basis. For example, if a given grain displays the activation of two prismatic slip systems and one pyramidal ⟨c + a⟩ slip system, this will result in three entries in the table. Examination of this table reveals that, as expected,

Table 2
Chemical composition of the raw materials (wt.%).

(a) CP Ti

O	V	Fe	C	Al	N	H	Ti
0.25	<0.09	<0.025	0.01	<0.01	0.0069	0.0008	Balance

(b) Ti–5Al–2.5Sn

Al	Sn	Fe	Zn	Ti
4.7	2.7	0.2	0.1	Balance

as the global Schmid factor decreases, the number of observed deformation systems of a given type generally decreases. It also suggests that some deformation system types, such as basal slip, are more likely to be activated than others, such as pyramidal ⟨c + a⟩. This is not a surprising observation since the CRSS is expected to be different for different deformation systems. Mitigating these apparent biases of one deformation system over another in assessing CRSSs is complicated by the fact that a given microstructural patch of grains also possesses an underlying texture. Consequently, some deformation systems will be oversampled in the deformation system–Schmid factor distribution if there are preferred orientations that have a particularly high Schmid factor for a given system.

It is the goal of the following section to develop an approach for removing these inherent biases and, as a result, deduce the underlying relative CRSS for the different deformation types. This is done by comparing the experimentally developed deformation system–Schmid factor distribution tables to theoretically developed tables based on the orientation distributions of the experimentally characterized microstructural patches.

3.2. Methodology for calculating the relative CRSS for the different slip system types

In this section a methodology for calculating the ratios of the CRSS for the various deformation system types is presented, based on the experimental observations of the activation of the different deformation system types. In Section 3.2.1, the manner for determining the total number of possible deformation systems for all the grains in a given microstructural patch is developed. The relative activation of the different deformation system types is then determined by comparing the potentially-activated systems to the experimentally-observed systems. In Section 3.2.2, an approach for taking into account the likelihood of deformation system activation as a function of the global Schmid factor is developed, incorporating the distribution of grain orientations in the microstructural region of interest. This results in prediction of the activation distribution of the different deformation system types for the given microstructural patch, under the assumption that all of the deformation system types have the same CRSS (which is clearly not the case). Finally, in Section 3.2.3, the results of Section 3.2.2 are compared to the experimentally observed activation distribution, and through a least-squares optimization procedure the approximate relative CRSSs of the different deformation system types are determined, so that the results of Section 3.2.2 are modified to mimic the experimental observations.

3.2.1. Comparison between the experimentally-observed deformation system activation distribution and the texture distribution

The Ti–5Al–2.5Sn tested in tension at ambient temperature will continue to be used as an example to illustrate the method. Table 4 lists the number of possible slip systems of a given deformation type and Schmid factor bin for all of the 147 grains in the EBSD mapped region, again based on a global uniaxial stress state, regardless of whether or not the deformation system was activated. For each hcp α grain, there are 24 possible slip systems, including 3 basal slip, 3 prismatic slip, 6 pyramidal ⟨a⟩ and 12 pyramidal ⟨c + a⟩ slip systems. Since dislocation slip is bidirectional, for the 24 slip systems in each of the 147 grains, the absolute value of the Schmid factor was computed for each grain, yielding 3528 values. However, since T1 twinning

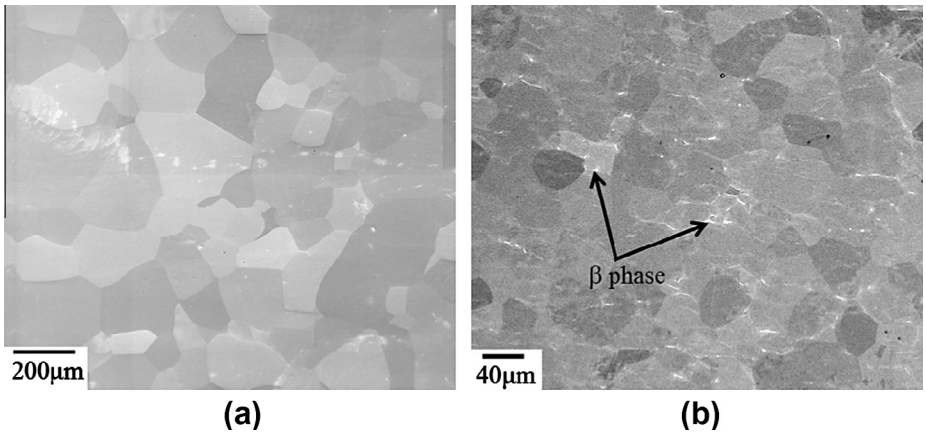

Fig. 1. (a) Secondary electron SEM photomicrograph of the as-received CP Ti; (b) backscattered electron SEM photomicrograph of the as-forged Ti–5Al–2.5Sn. The β phase (light phase) decorated the equiaxed α phase (dark phase) grain boundaries.

Table 3
Experimentally observed deformation system–Schmid factor distribution of the Ti–5Al–2.5Sn RT tension test.

Schmid factor	Basal	Prism	Pyra a	Pyra c + a	Twin
0–0.05	0	1	0	0	0
0.05–0.1	0	3	0	0	0
0.1–0.15	0	2	0	0	0
0.15–0.2	0	8	0	0	0
0.2–0.25	0	7	0	0	0
0.25–0.3	5	13	0	0	1
0.3–0.35	5	11	0	1	0
0.35–0.4	18	16	1	1	0
0.4–0.45	25	16	2	1	1
0.45–0.5	32	24	4	6	0

is unidirectional, each of the 6 possible T1 twin systems in each grain was counted only if it had a positive Schmid factor, yielding an additional 534 values, or a total of 4062 potential deformation systems distributed in Table 4, which we henceforth refer to as a potential deformation system–Schmid factor distribution. The data in Table 4 are binned in the same manner as described for Table 3, defined so that a particular Schmid factor range and deformation type can be uniquely denoted D_{ij}. In comparison, 204 deformation systems were actually observed, as seen in Table 3.

The experimentally observed deformation system–Schmid factor distribution is compared with the potential deformation system–Schmid factor distribution by dividing each pair in Table 3 (N_{ij}) with the corresponding pair in Table 4 (D_{ij}), resulting in:

$$\omega_{ij} = N_{ij}/D_{ij}. \quad (1)$$

This new Table 5 is called a deformation system–Schmid factor activation ratio distribution, with ω_{ij} representing the ratio of the number of observed deformation systems of type j with Schmid factor bin i to the corresponding potential number. If all the deformation systems represented in Table 4 were actually activated in the experiment, the value of each pair ω_{ij} in Table 5 would be 1, but this is clearly not the case. This deviation from a value of 1 in each Table 5 entry results from two reasons. First, because the activation of a particular deformation system depends on the resolved shear stress on the given deformation system, we expect that a deformation system with a small Schmid factor (i.e. small resolved shear stress) is less likely to be activated than one with a large Schmid factor. Therefore, it is no surprise that the ω_{ij} associated with low Schmid factors in Table 5 are much smaller than for high Schmid factors. Second, since we expect the CRSS values of the five deformation systems to be different, different deformation systems subjected to the same resolved shear stress should have different levels of activity. This feature in the data is observed by comparing pairs of ω_{ij} within the same row (same Schmid factor bin) of Table 5. For example, Table 5 suggests that the CRSS of basal slip is much smaller than pyramidal $\langle c + a \rangle$ slip for the Ti–5Al–2.5Sn ambient tension test. In Section 3.2.3, a CRSS ratio optimization process will be developed so that the difference between the number of experimental observations of the five deformation system types and the modified number of deformation systems based on the EBSD data is minimized.

3.2.2. Prediction of deformation system activation assuming the CRSS is the same for all deformation systems

Table 4 categorizes the number of potentially-activated deformation systems of a given deformation system type and Schmid factor range in a given microstructural patch for the ambient temperature tested Ti–5Al–2.5Sn sample. However, as stated in the analysis of Table 5 in Section 3.2.1, it does not represent the number of likely-activated deformation systems, which varies based on Schmid factor and deformation type. Using Table 5 as a guide, we now reduce the values in Table 4 associated with low Schmid factors and convert Table 4 to a table that reflects the relative importance of the Schmid factor on the deformation activity but still assumes that the CRSS is the same for all of the deformation system types. The results of Table 5 are plotted in Fig. 2 showing the activation ratio of the different deformation system types as a function of the global Schmid factor, which can be fitted using a cubic weighting function:

$$W_{ij} = D_{ij} \times ((i-1)/9)^3, \quad (2)$$

resulting in Table 6, which will be referred to as a weighted deformation system–Schmid factor distribution. This weighting function will not change the relative potential activation of the deformation systems associated with the highest Schmid factor value 0.45–0.5 (in Eq. (2), when $i = 10$, $W_{ij} = D_{ij}$, and the values in the bottom row of Table 6 are unchanged from Table 4), but will strongly suppress the potential activation of the deformation systems with smaller Schmid factors (i.e. for small i, since only a very small number of deformation systems with low Schmid factors are expected to be activated, the values in the first row of Table 6 are zero – consistent with those in Table 5 and much lower than those in Table 4). It should be noted that different scaling functions of the form in Eq. (2) may be more applicable for different metals and/or different deformation systems. Nevertheless, in this study, a

Table 4
Potential deformation system–Schmid factor distribution for all the grains in the EBSD mapped region of the Ti–5Al–2.5Sn RT tension test.

Schmid factor	Basal	Prism	Pyra a	Pyra c + a	Twin
0–0.05	57	81	178	264	64
0.05–0.1	54	66	106	244	55
0.1–0.15	56	54	103	195	62
0.15–0.2	38	60	87	164	52
0.2–0.25	40	37	92	180	59
0.25–0.3	40	44	82	137	66
0.3–0.35	31	23	61	148	59
0.35–0.4	45	28	71	154	58
0.4–0.45	44	21	44	151	36
0.45–0.5	36	27	58	127	23

Table 5
Deformation system–Schmid factor activation ratio distribution of the Ti–5Al–2.5Sn RT tension test.

Schmid factor	Basal	Prism	Pyra a	Pyra c + a	Twin
0–0.05	0	0	0	0	0
0.05–0.1	0	0.05	0	0	0
0.1–0.15	0	0.04	0	0	0
0.15–0.2	0	0.13	0	0	0
0.2–0.25	0	0.19	0	0	0
0.25–0.3	0.13	0.30	0	0	0.02
0.3–0.35	0.16	0.48	0	0.01	0
0.35–0.4	0.40	0.57	0.01	0.01	0
0.4–0.45	0.57	0.76	0.05	0.01	0.03
0.45–0.5	0.89	0.89	0.07	0.05	0

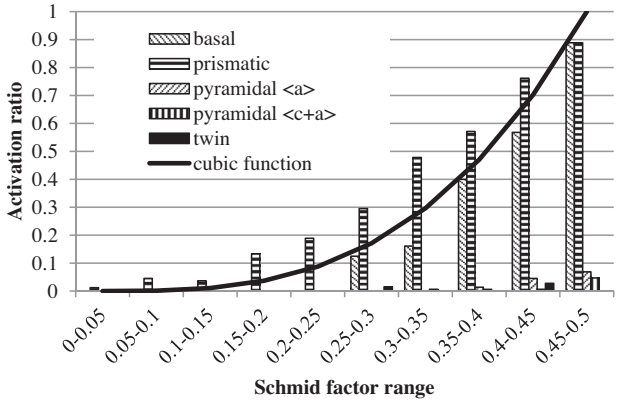

Fig. 2. Activation fraction vs. Schmid factor for the different deformation system types for Ti–5Al–2.5Sn tensile tested at RT, with the cubic parabola function overlaid.

number of different polynomial functions were tested, including quadratic, cubic, and fourth-order weighting functions, and there was no significant effect on the final results. In the present study, the cubic weighting function (Eq. 2) is used.

Based on the weighted deformation system–Schmid factor distribution in Table 6, an approximate probability density function is generated using:

$$p_{ij} = W_{ij} \Big/ \sum_{i,j} W_{ij}, \tag{3}$$

which, as shown in Table 7, represents the approximate probability of having deformation j with Schmid factor bin i activated, again assuming the CRSSs of all the deformation systems are the same. This approximate probability density function now allows the prediction of the expected number of observations of deformation system type j and Schmid factor bin i, denoted by P^0_{ij}, for any given total number of deformation systems S to be determined via:

$$P^0_{ij} = p_{ij} S. \tag{4}$$

For the Ti–5Al–2.5Sn RT tension test, a total of 204 deformation systems were observed ($S = \sum_{i,j} N_{ij} = 204$). So in this case P^0_{ij} represents the expected number of observations of a given deformation type j and Schmid factor bin i based on the probability density function generated in Eq. (3) if the total number of deformation systems were 204, as shown in Table 8. This table contains the expected number of activated deformation systems for the given texture of the microstructural patch assuming the CRSSs are the same for all the deformation system types. Note that the total number of observed deformation systems will vary for a given experimentally-characterized microstructural patch, testing condition, and material.

3.2.3. Optimization of CRSS ratio

The procedures in Section 3.2.2 do not consider the CRSS differences of the five deformation system types, and hence the experimentally-observed deformation system–Schmid factor distribution (N_{ij}) in Table 3 is significantly different from the expected distribution (P^0_{ij}) in Table 8. The next step is to optimize the CRSS ratios of the five deformation system types so that the difference between the experimental observations and the expected values is minimized. In this section, a methodology for determining the CRSS ratio is presented. This methodology involves a modification of P^0_{ij} (in Table 7, assuming CRSS is the same) using hypothetical CRSS values and least-square minimization to match the modified P^0_{ij} with the experimentally observed deformation system–Schmid factor distribution (N_{ij}) in Table 3.

Let τ_j denote the true CRSS of deformation system type j and P_{ij} the number of observations of deformation system type j and Schmid factor bin i, where it is not assumed that the CRSSs are identical. Then the expected number of observations of deformation system type j and Schmid factor bin i in Table 8, where it was assumed that the CRSSs are identical, can be related to this modified number P_{ij} via:

$$P_{ij} = \frac{c}{\tau_j} P^0_{ij}, \tag{5}$$

where c is an unknown constant with units of MPa. If the CRSS for one slip system type has been experimentally measured, the constant c can be determined, allowing the actual CRSSs to be determined for all of the other deformation system types. Nevertheless, this is not the case in

Table 6
Weighted potential deformation system–Schmid factor distribution for all the grains in the EBSD-mapped region of the Ti–5Al–2.5Sn RT tension test.

Schmid factor	Basal	Prism	Pyra a	Pyra c + a	Twin
0–0.05	0	0	0	0	0
0.05–0.1	0.07	0.09	0.15	0.33	0.08
0.1–0.15	0.61	0.59	1.13	2.14	0.68
0.15–0.2	1.41	2.22	3.22	6.07	1.93
0.2–0.25	3.51	3.25	8.08	15.80	5.18
0.25–0.3	6.86	7.54	14.06	23.49	11.32
0.3–0.35	9.19	6.81	18.07	43.85	17.48
0.35–0.4	21.17	13.17	33.41	72.46	27.29
0.4–0.45	30.90	14.75	30.90	106.05	25.28
0.45–0.5	36	27	58	127	23

the present analysis, so only the ratios of the CRSSs of the different deformation systems will be determined, and c was set to 1 MPa. Note that if all of the CRSSs are identical, i.e.

$$\tau_1 = \tau_2 = \tau_3 = \tau_4 = \tau_5 = c, \tag{6}$$

then the modified number of observations P_{ij} agree with the expected values given in Table 8. Alternatively, if $\tau_j > \tau_k$, then the modified number of observations P_{ij} for deformation system j is related to the analogous quantity P_{ik} for deformation system k by:

$$\frac{P_{ik}}{P^0_{ik}} = \frac{\tau_j}{\tau_k}\frac{P_{ij}}{P^0_{ij}} \tag{7}$$

so that the modified number of observations (relative to the expected number if the CRSSs are identical) in deformation system k is greater than the same relative number in deformation system j. This is consistent with deformation system k having a smaller CRSS than deformation system j.

The squared difference d between the number of experimental observations of each pair N_{ij} in Table 3 and the corresponding modified predicted number of observations P_{ij} is given by:

$$d(\tau_1,\tau_2,\tau_3,\tau_4,\tau_5;c) = \sqrt{\sum_{i,j=1}^{10,5}(P_{ij}-N_{ij})^2} = \sqrt{\sum_{i,j=1}^{10,5}\left(\frac{c}{\tau_j}P^0_{ij}-N_{ij}\right)^2}. \tag{8}$$

The "optimal" values for the CRSS values are then computed by solving the first-order derivative conditions for d with respect to τ_1, τ_2, τ_3, τ_4 and τ_5 (treating c as an unknown parameter) and using the result to minimize d:

$$\frac{\partial d}{\partial \tau_j} = 0 \rightarrow \tau^*_j = c\frac{\sum_{i=1}^{m}(P^0_{ij})^2}{\sum_{i=1}^{m}N_{ij}P^0_{ij}}, \tag{9}$$

where $\tau^*_1, \tau^*_2, \tau^*_3, \tau^*_4$, and τ^*_5 are the "optimal" CRSS values for basal, prismatic, pyramidal ⟨a⟩, pyramidal ⟨c + a⟩, and T1 twin deformation systems, respectively. In Eq. (9), although c is an unknown constant, the CRSS ratio of any two deformation systems will not depend on c. Thus, the CRSS ratios of the basal, prismatic, pyramidal ⟨a⟩, pyramidal ⟨c + a⟩ and T1 twin systems are given as:

$$\text{basal} : \text{prismatic} : \text{pyramidal}\ \langle a\rangle : \text{pyramidal}\ \langle c+a\rangle : \text{T1 twin} = \frac{\tau^*_1}{\tau^*_1} : \frac{\tau^*_2}{\tau^*_1} : \frac{\tau^*_3}{\tau^*_1} : \frac{\tau^*_4}{\tau^*_1} : \frac{\tau^*_5}{\tau^*_1}. \tag{10}$$

For the Ti–5Al–2.5Sn tested at RT, the estimated ratios are 1:0.79:15.5:30.1:54.5 for basal: prismatic: pyramidal ⟨a⟩: pyramidal ⟨c + a⟩: T1 twin. Using the above CRSS ratios, the predicted number of observations for a given deformation type j and Schmid factor bin i (P_{ij}) in Eq. (5) is shown in Table 9. Comparison of this table with the experimental results in Table 3 shows good general agreement.

The same methodology discussed in Sections 3.1–3.2 was employed to calculate the CRSS ratios for the CP Ti and Ti–5Al–2.5Sn tested at RT and 455 °C, strained to approximately 4% (and also about 10%) plastic deformation, and the significance of these values will be discussed next.

Table 7
Probability density function of the Ti–5Al–2.5Sn RT tension test.

Schmid factor	Basal	Prism	Pyra a	Pyra c + a	Twin
0–0.05	0	0	0	0	0
0.05–0.1	0.0001	0.0001	0.0002	0.0004	0.0001
0.1–0.15	0.0007	0.0007	0.0013	0.0025	0.0008
0.15–0.2	0.0016	0.0026	0.0037	0.0070	0.0022
0.2–0.25	0.0041	0.0038	0.0094	0.0183	0.0060
0.25–0.3	0.0080	0.0088	0.0163	0.0273	0.0131
0.3–0.35	0.0107	0.0079	0.0210	0.0509	0.0203
0.35–0.4	0.0246	0.0153	0.0388	0.0841	0.0317
0.4–0.45	0.0359	0.0171	0.0359	0.1231	0.0293
0.45–0.5	0.0418	0.0313	0.0673	0.1474	0.0267

Table 8
Expected activated deformation system–Schmid factor distribution of the Ti–5Al–2.5Sn RT tension test with a total of 204 deformation systems assuming CRSSs are the same for all the deformation system types.

Schmid factor	Basal	Prism	Pyra a	Pyra c + a	Twin
0–0.05	0	0	0	0	0
0.05–0.1	0.02	0.02	0.03	0.08	0.02
0.1–0.15	0.15	0.14	0.27	0.51	0.16
0.15–0.2	0.33	0.53	0.76	1.44	0.46
0.2–0.25	0.83	0.77	1.91	3.74	1.23
0.25–0.3	1.62	1.79	3.33	5.56	2.68
0.3–0.35	2.17	1.61	4.28	10.38	4.14
0.35–0.4	5.01	3.12	7.91	17.16	6.46
0.4–0.45	7.32	3.49	7.32	25.11	5.99
0.45–0.5	8.52	6.39	13.73	30.07	5.45

4. Results and discussion

One expects that if the same experiment were to be repeated numerous times on a patch of the same material (e.g. same texture, temperature, strain), the set of observed activated deformation systems would be slightly different than that given in Table 3 since each set of observations would represent a sample from the same population (and therefore with the same probability distribution). Therefore, the specific numbers computed using the observations in Table 3 and represented in Eq. (10) are only an estimate of the CRSS ratios, not the true CRSS ratios. Indeed, since the computed CRSS ratios depend on all of the data in Table 3, without further experiments it is not possible to explicitly compute additional estimates of the CRSS ratios. Despite this limitation, however, the accuracy of the CRSS ratio estimates computed using the method of Sections 3.1–3.2 and given in Eq. (10) can be assessed in two fundamental ways. First, the statistical resampling technique of

bootstrapping allows the generation a large number of pseudo datasets in order to simulate the repetition of numerous deformation experiments, compute the optimal set of CRSS ratios for each dataset, and then determine the corresponding mean CRSS ratios from this collection [33,34]. We can then use these averaged values as a more robust measure of true CRSS ratios, thereby facilitating discussion of the relationship between the mean CRSS ratios, the experimental data and the relevant values in the literature. Second, using the resampling distribution as an estimate of the true CRSS ratio distribution, we can compute rough confidence intervals for the CRSS ratios and analyze their corresponding significance.

4.1. Statistical analysis

For each of the experiments considered in this work (CP Ti and Ti–5Al–2.5Sn at RT and 455 °C, strained to approximately 4% and 10% plastic deformation), the bootstrapping analysis described below was followed.

1. Treating each experimental observation of deformation as an independent and identically distributed random variable, the raw experimental data (e.g. Table 3) was used to construct a discrete probability distribution $f_{ij} = N_{ij}/N$, where N_{ij} is the number of observations of deformation with Schmid factor bin i and deformation type j, and $N = \sum_{i,j=1}^{10,5} N_{ij}$ is the total number of deformation system observations for the experiment under consideration. Here f_{ij} represents an empirical probability distribution for all possible Schmid factor bins and deformation types, constructed by assigning a probability of $1/N$ to each experimental observation, regardless of Schmid factor bin or deformation type.
2. M pseudo data sets (each corresponding to a simulated experiment) were constructed by randomly sampling (with replacement) the observation sample space using the distribution f_{ij}, which represents the empirical probability that a given observation will lie in Schmid factor bin i and be of deformation type j. Each of the M data sets consisted of N "observations".
3. For each of the M pseudo data sets, the optimization problem from Section 3 was solved to deduce CRSS ratio estimates of the form given in Eq. (10).
4. Each of the generated populations of CRSS ratios were analyzed statistically by computing the mean and confidence intervals using the resampling distribution.

Fig. 3 depicts how this method was applied to the data in Table 3 for the Ti–5Al–2.5Sn strained 3.5% at RT. The resulting resampled CRSS ratio distributions are depicted in Fig. 4. Corresponding mean values, standard errors, and confidence intervals were then computed from these simulated distributions [35]. The mean values of the CRSS ratios for all bootstrapped pseudo data sets are given in Tables 10–12. Unless otherwise stated, the subsequent discussion refers to these mean values. The significance of the confidence intervals contained in Table 12 will be discussed in Section 4.5.

Table 9
Predicted activated deformation system–Schmid factor distribution of the Ti–5Al–2.5Sn RT tension test with a total of 204 deformation systems using optimized CRSS ratios.

Schmid factor	Basal	Prism	Pyra a	Pyra c + a	Twin
0–0.05	0	0	0	0	0
0.05–0.1	0.06	0.10	0.01	0.01	0.00
0.1–0.15	0.52	0.63	0.06	0.06	0.01
0.15–0.2	1.18	2.35	0.17	0.17	0.03
0.2–0.25	2.94	3.43	0.44	0.44	0.08
0.25–0.3	5.75	7.97	0.76	0.65	0.17
0.3–0.35	7.70	7.20	0.98	1.22	0.27
0.35–0.4	17.75	13.92	1.81	2.02	0.42
0.4–0.45	25.91	15.59	1.68	2.95	0.39
0.45–0.5	30.19	28.54	3.14	3.53	0.35

4.2. Comparison of the analysis of mean CP Ti CRSS ratios at ambient temperature with previous results

The calculated CRSS ratios of the CP Ti tested at RT are consistent with the prior work, indicating the validity of this technique. In Table 10, the calculated prismatic/basal CRSS ratio is 0.28, which is close to the value of 0.2 reported by Wu et al. [8]. This ratio has also been reported from other studies, with a wide range of 0.2–1.35 shown in Table 1. Pyramidal slip systems exhibited much higher mean CRSS values relative to basal (7.1 for pyramidal ⟨a⟩, 6.3 for pyramidal ⟨c + a⟩), which are similar to those reported in Ref. [1] and used in Ref. [11]. Furthermore, the CP Ti exhibits a moderate resistance to twinning (CRSS ratio = 1.7) among all of the deformation system types, which is larger than prismatic slip (0.28) but smaller than pyramidal ⟨a⟩ (7.1) and pyramidal ⟨c + a⟩ slip (6.3). This is also consistent with the prior observations that indicated that twinning is frequently observed for CP Ti and that the observed activity was less than that for prismatic and basal slip but more than that for pyramidal slip systems [21,24,36].

4.3. Analysis of the effect of alloy composition and deformation temperature on the CRSS ratios at low strain

In this section, the relative activity of the different deformation systems changes with alloying composition and deformation temperature are compared at low strain. Examination of Table 10 allows several statements to be made. Comparisons of the mean prismatic/basal CRSS ratios determined for RT shows that while prismatic slip is strongly favored in CP Ti (0.28), prismatic slip becomes less favorable in the alloy (0.81). The lower resistance of prismatic slip relative to basal slip is unaffected by temperature for CP Ti (prismatic/basal CRSS ratios of 0.28 and 0.29, respectively). In contrast, for the Ti–5Al–2.5Sn alloy, similar analysis suggests that basal slip becomes less

favorable (0.81) to more favorable (1.17) with increasing deformation temperature. These trends agree with earlier observations, indicating that prismatic slip is favored in unalloyed Ti and that basal activity increases with Al additions and temperature [21].

The activity of the other deformation systems relative to the activity of basal slip is also affected by alloying and temperature. With increasing temperature for CP Ti, the relative CRSS of pyramidal ⟨a⟩ and pyramidal ⟨c + a⟩ slip decreases slightly for CP Ti (7.1 and 6.3 at RT, 5.4 and 4.7 at 455 °C). For Ti–5Al–2.5Sn, a similar decrease in the activity of pyramidal ⟨a⟩ and pyramidal ⟨c + a⟩ slip was also observed with increasing temperature. Overall, the mean pyramidal/basal CRSS ratio in CP Ti (4.7–7.1) is much lower than for Ti–5Al–2.5Sn (16.7–35.5).

The relative activity of twinning also changes with alloying and temperature. For the CP Ti, twinning is an active deformation system at both RT and 455 °C, and the relative activity of twinning is not significantly affected by temperature (1.7 at ambient temperature, 1.8 at 455 °C). However, Ti–5Al–2.5Sn exhibits a very high resistance to twinning (74) among all the other deformation systems at RT. Furthermore, as twinning was not observed in the Ti–5Al–2.5Sn at elevated temperature, no CRSS ratio value was calculated. This low twinning activity in Ti–5Al–2.5Sn is consistent with the observations of Williams et al. [21] where it was reported that twinning can be restricted by the ordering of Al in the α phase and that twinning can be further suppressed with increasing temperature for Ti–Al alloys.

The present work ignores any influences that the β phase may have on the mechanical response of the microstructure and how such influences may affect the deformation response of the α phase. As the β phase makes up less than 1% of the microstructure of the Ti–5Al–2.5Sn alloy, it may be reasonable to assume that the β phase of the Ti–5Al–2.5Sn alloy does not significantly affect the relationship between the activation of deformation in the α phase and the associated CRSSs. This is confirmed by recent crystal plasticity finite-element modeling of a Ti–5Al–2.5Sn microstructure patch, which shows that the small amount of β at the α grain boundaries does not alter the local stress state significantly when compared to the same microstructure patch simulated without the grain boundary phase [38].

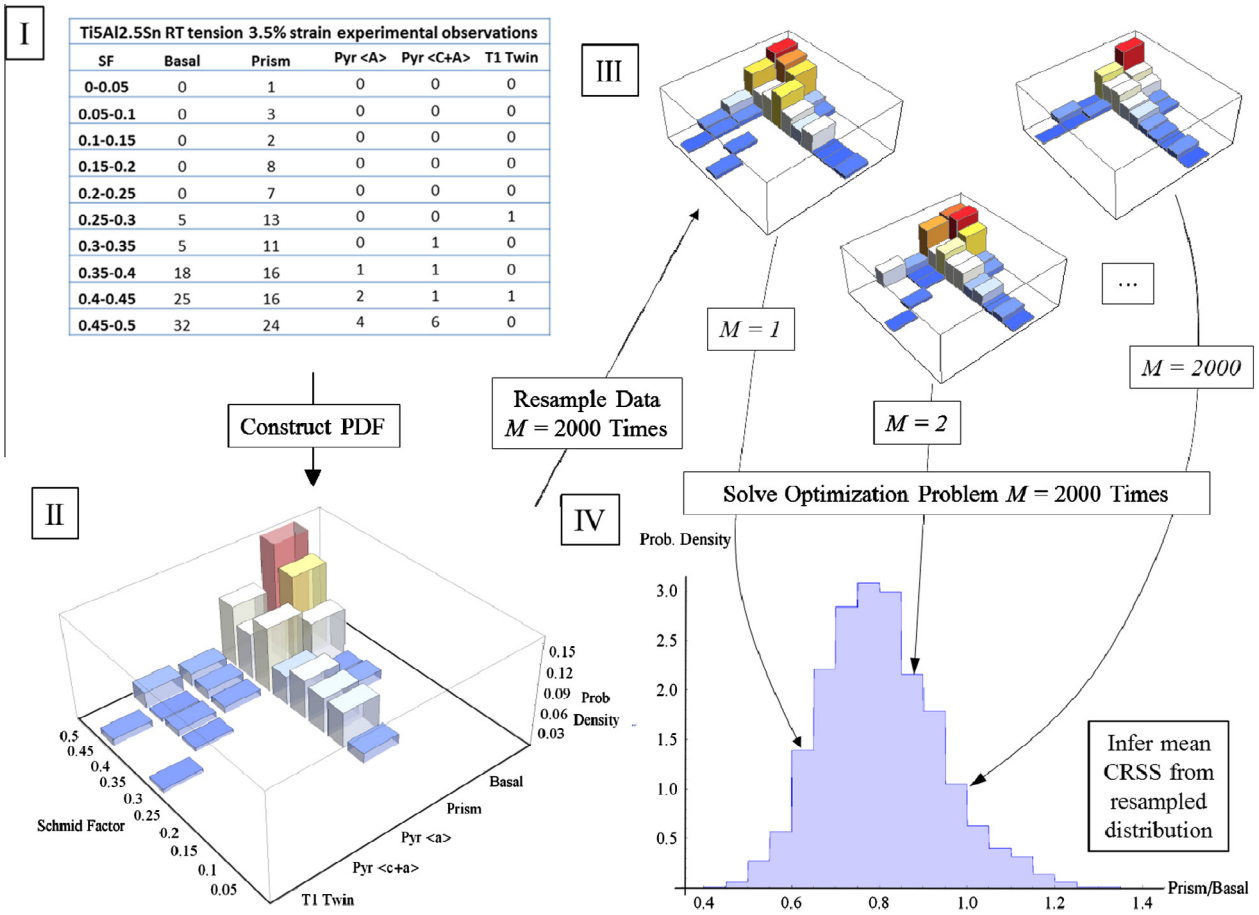

Fig. 3. The bootstrap method applied to computing CRSS ratios for Ti–5Al–2.5Sn tensile tested at RT to 3.5% strain. (I) Original experimental observations. (II) Probability density function (PDF) constructed directly from observations. (III) Exemplar pseudo dataset resulting from one possible sample of the PDF given in (II). (IV) Probability density function constructed from the optimal prismatic/basal CRSS ratios that result from 2000 resamples of the original dataset in (I).

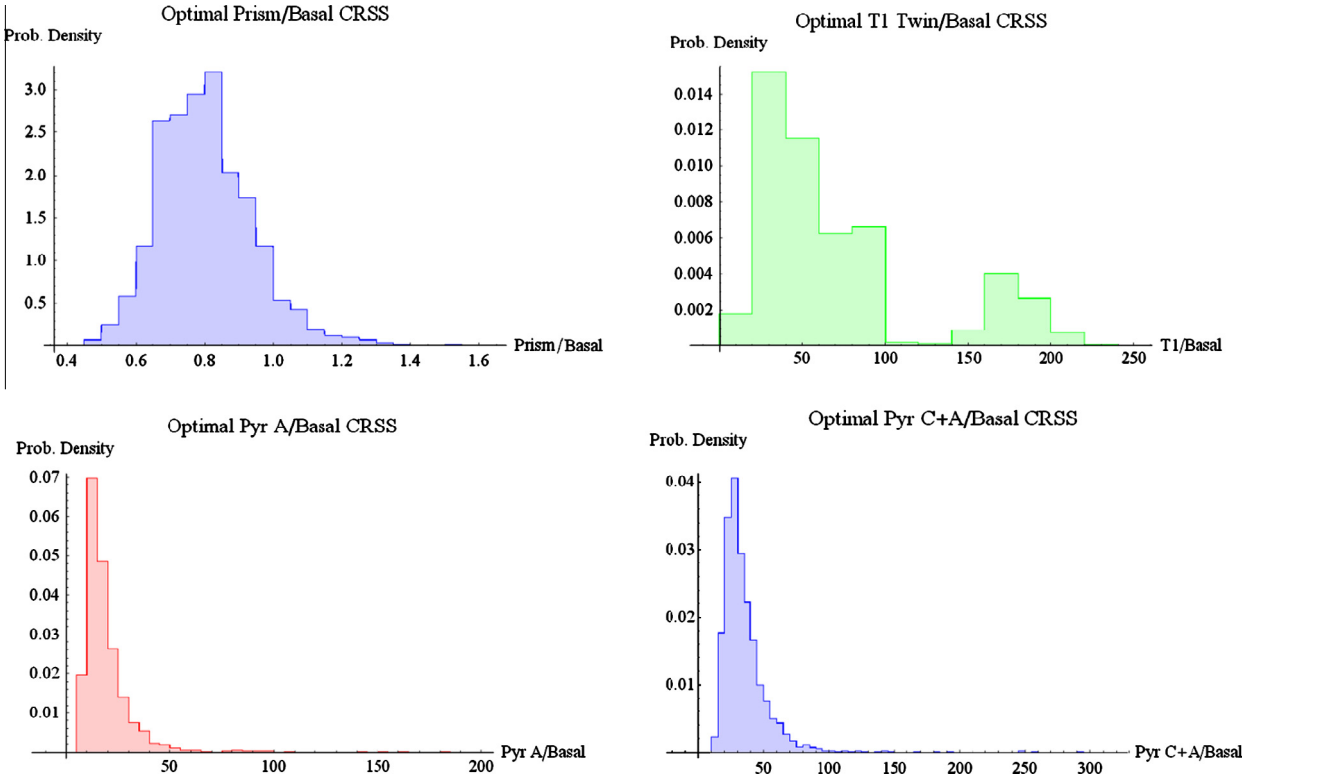

Fig. 4. Resampling probability density functions for Ti–5Al–2.5Sn tensile tested at RT to 3.5% strain. The second low peak in the T1 twin/basal CRSS ratio is due to the existence of only two T1 twin observations with different Schmid factors. Although the pyramidal ⟨a⟩/basal and pyramidal ⟨c + a⟩/basal CRSS ratio distributions exhibit overlap, the populations also are nevertheless visually distinct.

Table 10
Bootstrapped mean CRSS ratios of basal, prismatic, pyramidal ⟨a⟩, pyramidal ⟨c + a⟩ and T1 twin deformation systems for CP Ti and Ti–5Al–2.5Sn tested at RT and 455 °C with approximately ~4% plastic deformation. * Twinning was not observed for Ti–5Al–2.5Sn tested at 455 °C.

Materials	Testing temperature	Strain (%)	Basal	Prismatic	Pyramidal ⟨a⟩	Pyramidal ⟨c + a⟩	T1 twin
CP Ti	Ambient	4	1	0.28	7.1	6.3	1.7
CP Ti	455 °C	4.3	1	0.29	5.4	4.7	1.8
Ti–5Al–2.5Sn	Ambient	3.5	1	0.81	19.1	35.5	74
Ti–5Al–2.5Sn	455 °C	4.4	1	1.17	16.7	24.4	*

Table 11
Bootstrapped mean CRSS ratios of basal, prismatic, pyramidal ⟨a⟩, pyramidal ⟨c + a⟩ and T1 twin deformation systems for CP Ti at RT and 455 °C and Ti–5Al–2.5Sn at 455 °C with ~10% plastic deformation. * Twinning was not observed for Ti–5Al–2.5Sn tested at 455 °C.

Materials	Testing temperature	Strain (%)	Basal	Prismatic	Pyramidal ⟨a⟩	Pyramidal ⟨c + a⟩	T1 twin
CP Ti	Ambient	4	1	0.28	7.1	6.3	1.7
CP Ti	Ambient	8.4	1	0.32	9.2	4.6	2.2
CP Ti	455 °C	4.3	1	0.29	5.4	4.7	1.8
CP Ti	455 °C	11.2	1	0.23	4.2	3.9	1.2
Ti–5Al–2.5Sn	455 °C	4.4	1	1.17	16.7	24.4	*
Ti–5Al–2.5Sn	455 °C	9	1	0.83	14.1	19.2	*

Another justification for ignoring the β phase is that the statistical approach used in the present work does not consider the geometry of the microstructure. That is, the orientations and mechanical responses of neighboring grains are not taken into account when identifying the activated deformation systems in a given grain. This lack of dependence on the local grain environment leads to the potential to use the method outlined here to assess the CRSS ratios of different phases in complex multiphase materials, if the effects of microstructural details average out with a sufficiently large population.

4.4. Analysis of the effect of strain on the CRSS ratios

As noted previously [28], with increasing strain more deformation systems were observed. For the CP Ti tested at RT and 455 °C and the Ti–5Al–2.5Sn tested at 455 °C, the activated deformation system data sets were collected at ~10% plastic strain. Using the same methodology as described in Section 4.1, the mean CRSS ratios were determined and are shown in Table 11. Some variation in the calculated ratios for a given set of alloy/temperature conditions as a function of strain is observed. For

Table 12
Bootstrapped mean CRSS ratios and their associated 90% confidence intervals. For each of the seven strain levels, the bootstrapped mean is listed above the corresponding 90% confidence interval. * Confidence intervals were not computed for T1 twins in the Ti–5Al–2.5Sn alloy at 455 °C due to a lack of observations.

Materials	Testing temperature	Strain (%)	Prismatic	Pyramidal ⟨a⟩	Pyramidal ⟨c + a⟩	T1 twin
			Basal	Basal	Basal	Basal
Means and 90% confidence intervals, in parenthesis						
CP Ti	RT	4	0.28	7.1	6.3	1.7
			(.12, .48)	(.81, 25.9)	(2.1, 13.1)	(.6, 3.5)
	455 °C	4.3	0.29	4.9	4.7	1.8
			(.14, .49)	(1.5, 11.4)	(2, 9.1)	(.6, 3.8)
	RT	8.4	0.32	9.2	2.3	1.3
			(.15, .53)	(2.4, 21.9)	(1.8, 8.5)	(.78, 4.4)
	455 °C	11.2	0.23	4.1	3.9	1.2
			(.11, .38)	(1.2, 9)	(1.7, 7.4)	(.48, 2.3)
Ti–5Al–2.5Sn	RT	3.5	0.81	19	35	74
			(.61, 1.05)	(8.7, 38.5)	(17.2, 65.2)	(21, 187)
	455 °C	4.4	1.17	16.7	24.4	*
			(.68, 1.85)	(1.96, 46.1)	(7.3, 72.9)	*
	455 °C	9	0.83	14.1	19.2	*
			(.6, 1.09)	(7, 26.3)	(10.7, 32.2)	*

example, when deformed at high temperatures, both the CP Ti and the Ti–5Al–2.5Sn show a decrease in the CRSS ratios for basal to prismatic slip from their RT values, decreasing from 0.29 to 0.23 and 1.17 to 0.83 respectively.

In addition to the statistical uncertainty discussed in Sections 4.1 and 4.5, there may be other reasons to expect the ratios to change as a function of strain. First, it is expected that as the polycrystalline samples deform, the individual grains will rotate. The resulting change in texture with deformation has not been accounted for in this methodology, with the texture corrections being based only on the texture in the undeformed state. Second, as the strain increases, some of the lower activity systems may become more evident and contribute to the deformation system–Schmid factor distributions (representing actual experimentally-observed deformation events first detailed in Table 3). As deformation continues, additional deformation on the systems initially observed in the deformation system–Schmid factor distribution is not quantified as changes to the table, but activation of additional deformation systems will be reflected in the deformation system–Schmid factor distribution. Third, while the current analysis assesses the Schmid factors relative to the global state of stress, the local state of stress varies to some degree due to the constraints of polycrystalline deformation [39–43]. These variations should average out with large data sets. Nevertheless, the biases associated with local deviations from the global state of stress are complex, and will evolve as the rate of deformation in neighboring grains varies. Finally, it is possible that the changes in the observed CRSS ratios with strain reflect a real change in materials behavior in that the work hardening for the different deformation system types is expected to be different [10,30,36,42,43], and, consequently, the stress necessary to activate these different systems will vary with strain. If this is in fact the case, the method developed here has the potential to allow assessment of these differences in work-hardening behavior, allowing access to the evolving work-hardening parameters critical to crystal plasticity finite-element models used for anisotropic deformation studies.

4.5. Statistical confidence and data resampling

The uncertainty inherent in the CRSS ratios computed in Section 3 is influenced by both non-systematic errors resulting from the choice of microstructural patch and sample sizes, as well as from systematic errors such as those that may result from the inability to identify certain deformation systems [28,37]. Although application of the bootstrap method discussed in Section 4.1 to the raw experimental data provides a robust way to estimate the mean CRSS ratios for various deformation system pairs in the CP Ti and the Ti–5Al–2.5Sn alloy, it cannot completely remove uncertainty in the original observations. Nevertheless, such uncertainty can be quantified using confidence intervals computed form the sampling distributions computed and displayed in Fig. 3 (part IV) and Fig. 4. Using the percentile method discussed in Ref. [35], $100(1-\alpha)\%$ confidence intervals of the form $(l_{\alpha/2}, r_{\alpha/2})$ were computed for the mean CRSS ratios. The endpoints $l_{\alpha/2}$ and $r_{\alpha/2}$ were deduced so that $(-\infty, l_{\alpha/2})$ contained the lowest $\alpha/2\%$ of the resampled data from the bootstrapping simulation and $(r_{\alpha/2}, \infty)$ contained the largest $(1-\alpha/2)\%$ of the resampled data. Note that such intervals are typically not symmetric about the distribution mean. 90% confidence intervals ($\alpha = 0.1$) and their corresponding means are given in Table 12. Based on this, a number of comparisons of the different pairs of CRSS ratios across experiments and deformation systems can be made, all with at least 90% confidence:

1. Under all conditions in CP Ti, the CRSS of prismatic slip is no more than 53% of the CRSS of basal slip. At RT and 4% strain the CRSS of pyramidal ⟨a⟩ slip is at least 81% of the CRSS of basal slip, but under all other conditions the CRSS of pyramidal ⟨a⟩ slip is at least 120% of the CRSS of basal slip.
2. At RT and low strain, the prismatic CRSS in CP Ti is no more than 48% of the basal CRSS in CP Ti, while in the Ti–5Al–2.5Sn alloy the prismatic CRSS is at least 68% of the CRSS for basal slip.
3. In CP Ti, changes in deformation temperature and strain do not significantly alter the prismatic-to-basal CRSS ratio.
4. While the mean prismatic to basal CRSS ratio in the Ti–5Al–2.5Sn alloy is 0.81 at low strain and RT, it is 1.17 at 455C, suggesting that the prismatic to basal CRSS ratio changes from favoring prismatic slip to favoring basal slip with increasing temperature. Although the confidence intervals do not support such a definitive statement, visual comparison of the resampling distributions in Fig. 5 does suggest that the mean prismatic to basal CRSS ratio at low temperature is significantly lower than at high temperature.
5. In Ti–5Al–2.5Sn at RT and 3.5% strain, the mean pyramidal-⟨a⟩ to-basal CRSS ratio (19) is considerably less than the mean pyramidal ⟨c + a⟩-to-basal CRSS ratio (35). Moreover, despite inconclusive confidence intervals, the resampled population distributions shown in Fig. 6 indicate a clear separation of the populations, supporting the hypothesis that pyramidal ⟨c + a⟩ slip is significantly more difficult to activate than pyramidal ⟨a⟩ slip in Ti–5Al–2.5Sn.

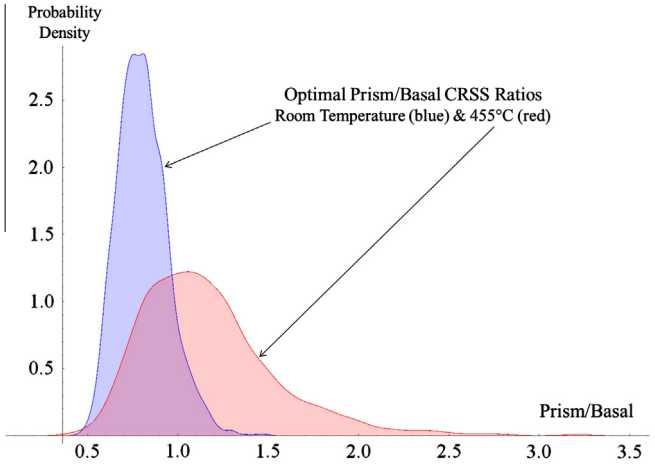

Fig. 5. Smoothed resampling probability density functions for Ti–5Al–2.5Sn tensile tested at both RT and 3.5% strain (blue), and at 455 °C and 4.4% strain (red). Although the spread in the densities prohibits a definitive statistical statement about the relative sizes of these ratios (see Table 11), a clear visual distinction between the two populations exists.

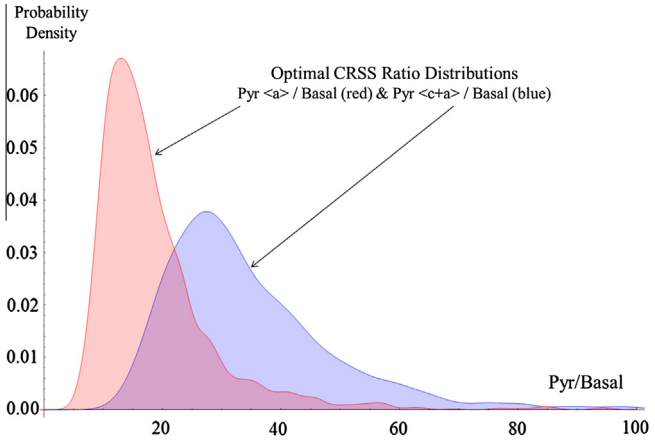

Fig. 6. Smoothed resampling probability density functions for the pyramidal ⟨a⟩/basal CRSS ratios (red) and the pyramidal ⟨c + a⟩ CRSS ratios (blue) in Ti–5Al–2.5Sn tensile tested at RT and 3.5% strain. The densities suggest that the CRSS ratio for pyramidal ⟨a⟩/basal is significantly less than the pyramidal ⟨c + a⟩/basal CRSS ratio.

4.6. Broader implications

Overall, the novel approach outlined here provides a flexible means to assess the CRSS for a variety of deformation systems, and has the potential to be applied to a wide range of alloys and crystal systems. When combined with the knowledge of specific CRSSs that are more easily obtained using more conventional methods, such as for the CRSS of prismatic slip in Ti, the absolute values of the CRSSs of slip systems with higher slip resistance can be determined. This technique allows these values to be determined over a wide range of temperatures, as long as the tests do not inhibit the observation of slip lines. Furthermore, this technique should be viable for determining CRSS ratios in multiphase materials, where most traditional approaches cannot be used. To date, the approach has also been shown to work well for the CRSS ratio estimation of Mg–rare earth alloys tested over a range of temperatures [44]. Access to these parameters has the potential to allow for more advanced modeling and understanding of materials behavior in the future.

It is important to note that the methodology presented in this work only identifies slip activity indirectly through the observation of surface slip traces. This approach has the potential to miss the activation of some deformation systems. First, slip systems with Burgers vectors parallel to the sample surface will not develop observable slip traces. Likewise, diffuse slip will not lead to well-defined slip bands. Furthermore, the deformation systems observed at the surface may not reflect the subsurface activity, as the nature of the constraint will change, which may affect the activation of the various deformation systems. It would be instructive to combine the methodology outlined here with subsurface characterization techniques, such as TEM or X-ray diffraction methods to determine if the surface observations accurately reflect the subsurface activity. These approaches could be used as a check for specific grain observations, but it would be difficult to carry out

enough observations to have the statistical robustness of the methodology presented here.

5. Summary

In this study, a methodology of calculating the CRSS ratios of polycrystalline metals has been developed and described. The CRSS ratios were determined by solving an optimization problem to minimize the difference between the experimentally-observed deformation system–Schmid factor distribution and the modified distribution based on the texture. The CRSS ratios of the CP Ti and Ti–5Al–2.5Sn in tension at RT and 455 °C were calculated using this methodology, with the results showing good agreement with literature data. It was found that the relative activity of the different deformation systems changes as a function of alloy composition and deformation temperature. With increasing plastic deformation, the CRSS variation at low and high strains has been observed, which may be the result of differently evolving hardening behavior in different slip systems, or other sources of uncertainty, which point toward valuable new areas for research related to statistical errors, rotations of grains during deformation and local stress state variation.

Acknowledgements

This research was supported by the US Department of Energy, Office of Basic Energy Science through Grant No. DE-FG02-09ER46637. The authors are grateful to Dr. P. Eisenlohr, previously at Max-Planck-Institut für Eisenforschung and currently at Michigan State University, for helpful discussions, and Mr. J. Seal and Mr. A. Chakkedath of Michigan State University, and Dr. Z. Chen, previously at Michigan State University and currently at Washington State University, for their assistance with the sample preparation and in situ tests. The authors are grateful to Mr. T. Van Daam of Pratt & Whitney, Rocketdyne for providing the Ti–5Al–2.5Sn alloy used in this study, and to Dr. C. Cowen, previously at National Energy Technology Laboratory, Albany, OR and currently at United States Mint, West Point, NY, who provided the CP Ti used in this study.

References

[1] Paton NE, Backofen WA. Metall Trans 1970;1:839.
[2] Shin DH, Kim I, Kim J, Kim YS, Semiatin SL. Acta Mater 2003;51:983.
[3] Yoo MH. Metall Trans A 1981;12A:409.
[4] Akhtar A. Metall Trans A 1975;6A:1105.
[5] Gong J, Wikinson AJ. Acta Mater 2009;57:5693.
[6] Paton NE, Williams JC, Rauscher GP. Titanium science and technology. In: Jaffee RI, Burte HM, editors. In: Proceedings of the second international conference. New York: Plenum Press; 1973.
[7] Zaefferer S. Mater Sci Eng A 2003;344:20.
[8] Wu X, Kalidindi SR, Necker C, Salem AA. Acta Mater 2007;55:423.
[9] Poty A, Raulot J-M, Xu H, Bai J, Schuman C. J Appl Phys 2011;110(014905):01.
[10] Salem AA, Kalidindi SR, Semiatin SL. Acta Mater 2005;53:3495.
[11] Balasubramanian S, Anand L. Acta Mater 2002;50:133.
[12] Jones IP, Hutchinson WB. Acta Metall 1981;29:951.
[13] Perilla M, Sevillano G. Mater Sci Eng A 1995;201:103.
[14] Bridier F, Villechaise P, Mendez J. Acta Mater 2005;53:555.
[15] Dick T, Cailletaud G. Comput Mater Sci 2006;38:113.
[16] Fundenberger JJ, Philippe MJ, Wagner F, Esling C. Acta Mater 1997;45:4041.
[17] Dunst D, Mecking H. Z Metallkd 1996;87:498.
[18] Lebensohn RA, Canova GR. Acta Mater 1997;45:3687.
[19] Bieler TR, Semiatin SL. Int J Plast 2002;18:1165.
[20] Feaugas X, Pilvin P, Clavel M. Acta Mater 1997;45:2703.
[21] Williams JC, Baggerly RG, Paton NE. Metall Mater Trans A 2002;33A:837.
[22] Chan KS. Metall Mater Trans A 2004;35:3409.
[23] Christian JW, Mahajan S. Prog Mater Sci 1995;39:1.
[24] Yang Y, Wang L, Bieler TR, Eisenlohr P, Crimp MA. Metall Mater Trans A 2011;42A:636.
[25] Conrad H. Prog Mater Sci 1981;26:123.
[26] Akhtar A, Teghtsoonian E. Metall Mater Trans 1975;6A:2201.
[27] Von Mises R, Angew Z. Math Mech 1928;8:161.
[28] Li H, Mason DE, Yang Y, Bieler TR, Crimp MA, Boehlert CJ. Philos Mag 2013;93:2875.
[29] ASTM. E112-96 Standard test methods for determining average grain size; 2004.
[30] Zambaldia C, Yang Y, Bieler TR, Raabe D. J Mater Res 2012;27:357.
[31] Yang Y. PhD dissertation. Michigan State University; 2011.
[32] Collins TJ. BioTechniques 2007;43:25.
[33] Effron B. Ann Stat 1979;7:1.
[34] Effron B. Biometrika 1981;68:589.
[35] Carpenter J, Bithell J. Stat Med 2000;19:1141.
[36] Wang L, Barabash RI, Yang Y, Bieler TR, Crimp MA, Eisenlohr P, et al. Metall Mater Trans A 2011;42A:626.
[37] Li H, Boehlert CJ, Bieler TR, Crimp MA. Philos Mag 2012;92:2923.
[38] Zhang C, Li H, Eisenlohr P, Liu W, Boehlert CJ, Crimp MA, Bieler TR., in preparation.
[39] Molinari A, Canova GR, Ahzi S. Acta Mater 1987;35:2983.
[40] Prakash A, Lebensohn RA. Model Simul Mater Sci Eng 2009;17:064010.
[41] Kanjarla AK, Houtte PV, Delannay L. Int J Plast 2010;26:1220.
[42] Kalidindi SR, Bhattacharyya A, Doherty RD. Proc Roy Soc Lond A 2004;49:1935.
[43] Kalidindi SR, Bronkhorst CA, Anand L. J Mech Phys Solids 1992;40:537.
[44] Ying DD, Wang QD, Boehlert CJ, Chen Z, Li H, Mishra RK., in preparation.